

Mass dependence in the production of light fragments in heavy-ion collisions

Jaivir Singh and Rajeev K. Puri

Department of Physics, Panjab University, Chandigarh 160 014, India

(Received 20 April 2001; published 11 January 2002)

Using the quantum molecular dynamics model coupled with the minimum spanning tree clusterization algorithm, we investigate the system-size effects in the production of light mass fragments (with mass ≤ 10). This was achieved by simulating the collision of symmetric nuclei like Ca+Ca, Ni+Ni, Nb+Nb, Xe+Xe, Er+Er, Au+Au, and U+U at incident energies between 50 MeV/nucleon and 1 GeV/nucleon and over full range of impact parameter. Our detailed analysis shows that the triggering of the multifragmentation and its saturation is delayed in heavier systems. The striking result, which is independent of the incident energy as well as of the impact parameter, is that the mass dependence of the multiplicity of any kind of fragment exhibits a power law behavior $\propto A_{tot}^\tau$, where “ A_{tot} ” is the mass of the composite system. Similar mass dependencies have already been reported in the literature for the fusion process at low incident energy as well as for the production of kaon and collective flow (and its disappearance) at intermediate energies. As reported for the production of kaons, the parameter τ depends on the colliding geometry as well as on the incident energy. No unique dependence of τ (such as, in the case of disappearance of flow) exists. The value of the parameter τ in central low energy collisions is close to 2/3, which suggests the dominance of the mean field. On the other hand, a linear dependence occurs at higher incident energies. Similar trends can also be seen in the preliminary reports of the FOPI experiments.

DOI: 10.1103/PhysRevC.65.024602

PACS number(s): 25.70.Pq, 24.10.Lx

I. INTRODUCTION

Does the mass of the system affect the dynamics? This question has always captured the central place in present day nuclear research. Ranging from the problems of nuclear structure to the decay of (excited) compound nucleus at low incident energies as well as the particle emission and its production at intermediate and high energies, the mass of the system is expected to play a dominant role. One has always tried to understand the system size effects in terms of scaling factors. At low incident energies, one has tried to understand the mass dependence, for instance, in the fusion process [1] where one concluded that the Coulomb force contributes significantly towards the barrier that can be parametrized in terms of the masses (and charges) of the colliding nuclei [1].

Similar efforts are also made at intermediate energies to pin down the system-size dependence in various phenomena. This includes the temperature as well as the density, nuclear flow of nucleons/fragments, disappearance of flow, particle production, multifragmentation, etc. The study of the mass dependence in the evolution of the density and temperature reveals that the maximum temperature is insensitive towards the mass of the system. However, the maximum density scales with the size of the interacting system [2–4]. As noted in Refs. [5,6], the reaction volume is much larger in heavier systems, which leads to significant higher average baryonic density.

Another interesting study (of the system size effect) was made for the particle production by Hartnack *et al.* [7] who found that the probabilities of the kaon production scale with the size of the system that can be parametrized in terms of a power law A_{tot}^τ ; A_{tot} is the mass of the composite system [7]. In a recent experiment [6], the KAOS group also reported the K^+ production per nucleon, which increases with the size of the system.

In another experimental analysis, the entropy of the system, however, was found to depend weakly on the size of the system [8]. The other signature of the compressional effects (predicted by the equation of state) is the collective flow. Its dependence on the mass of the colliding nuclei has been investigated extensively during last few years [4,9]. The balance energy at which the flow disappears depends strongly on the (composite) mass of the system ($\propto A_{tot}^{-1/3}$) [10].

In contrary, fewer attempts exist in the literature, which deal with the systematic study of the mass dependence in multifragmentation [11–16]. Most of the reported studies involve the asymmetric colliding nuclei at a fixed relative velocity [14,16]. The recent reports from the FOPI experiments [12] depict the dependence of the multiplicity of heavy fragments on the size of the interacting system. This was carried out for symmetric nuclei, such as, Ni+Ni, Ru+Ru, Xe+CsI, and Au+Au. In other words, the center-of-mass velocity is kept fixed in all these cases. Until recently, no systematic theoretical attempt was made to study the role of the masses of colliding nuclei in multifragmentation [17].

Note that the dynamics in light colliding nuclei can be quite different compared to heavy colliding nuclei. The surface contribution in light nuclei (like C, O, Ne, etc.) is much larger than in the heavy nuclei (like Pb, U, etc.). In other words, the surface to volume ratio (which depends on the size of the system) can play a vital role [4,5,11–14]. Further, as noted by several authors, the heavy nuclei can be compressed strongly, which may lead to faster expansion of the compressed matter [4,5]. This also points toward the relation between the production of intermediate mass fragments and the collective flow built during the compression [18]. It was noted in Ref. [14] that the initial radial kinetic energy of the composite system depends strongly on the initial compression-decompression dynamics that varies with the mass ratio of the target/projectile. Motivated by these find-

ings, we present here a complete study of the mass dependence in the production of light and medium mass fragments. We here model the symmetric reactions involving the nuclei with masses between 40 and 238. We shall show that the multiplicity of any fragment scales with the size of the interacting system that can be parametrized in terms of a power law function.

It is worth mentioning that the theoretical situation is rather complicated. There are several different models that can be applied to study the fragmentation. These models can be divided broadly into two groups.

(i) The models of the first group are based on the statistical approach [19]. These models neglect the dynamics of a reaction and hence depend on the (freeze-out) excitation energy and density of the composite system only. In other words, the nucleon-nucleon correlations are neglected and one cannot study the formation and origin of fragments.

(ii) The second type of models are the dynamical models that are capable of following the reaction from the start to the end where matter is cold and fragmented. In these models, one can study the formation and origin of the fragments on a microscopic level. In this category, the one body approach, such as, the Boltzmann-Uhling-Uhlenbeck model [20] and many body approach like the quantum molecular dynamics (QMD) model [5,21] are well known and widely used. One should, however, keep in the mind that the multifragmentation is a many body phenomena, therefore, molecular dynamical models are excellent tools to investigate the fragmentation. We shall carry the above study within the framework of the QMD model [5,21] which is discussed in brief in Sec. II. The results are presented in Sec. III and we summarize the results in Sec. IV.

II. QMD MODEL

The QMD model is a time dependent many body theory to simulate the time evolution of heavy ion reactions on an event-by-event basis. It is based on a generalized variational principle where one needs to choose the test wave function ϕ . In the QMD approach, the test wave function is an A_{tot} -body wave function with $6A_{tot}$ time dependent parameters [4,5,17,18,21,22].

To calculate the time evolution of the system we start out from the action

$$S = \int_{t_1}^{t_2} \mathcal{L}[\phi, \phi^*] dt, \quad (1)$$

with the Lagrange functional

$$\mathcal{L} = \left\langle \Phi \left| i\hbar \frac{d}{dt} - H \right| \Phi \right\rangle. \quad (2)$$

The total time derivative includes the derivation with respect to the parameters. The time evolution of these parameters is obtained by the requirement that the action is stationary under the allowed variation of the wave function. This leads to an Euler-Lagrange equation for each time dependent parameter.

The basic assumption of the QMD model is that a test wave function of the form

$$\Phi = \prod_{i=1}^{A_T+A_P} \phi_i, \quad (3)$$

with

$$\begin{aligned} \phi_i(\mathbf{r}, t) = & \left(\frac{2}{L\pi} \right)^{3/4} \exp\{-[\mathbf{r} - \mathbf{r}_i(t)]^2/4L\} \\ & \times \exp\{i[\mathbf{r} - \mathbf{r}_i(t)]\mathbf{p}_i(t)\} \exp[ip_i^2(t)t/2m], \quad (4) \end{aligned}$$

is a good approximation to the nuclear wave function. The time dependent parameters are $\mathbf{r}_i(t)$, $\mathbf{p}_i(t)$, and $L = 1.08 \text{ fm}^2$, which is fixed. In other words, the rms radius of a nucleon is about 1.8 fm and hence almost twice as large as that obtained from electron scattering. A smaller value of the L is excluded because the nuclei would become unstable after initialization. The present value of L represents the limit for a semiclassical theory. The influence of different Gaussian widths L in multifragmentation is reported in detail in Refs. [18,21].

The variation yields as

$$\dot{\mathbf{r}}_i = \frac{\mathbf{p}_i}{m} + \nabla_{\mathbf{p}_i} \sum_j \langle V_{ij} \rangle = \nabla_{\mathbf{p}_i} \langle H \rangle, \quad (5)$$

$$\dot{\mathbf{p}}_i = -\nabla_{\mathbf{r}_i} \sum_{j \neq i} \langle V_{ij} \rangle = -\nabla_{\mathbf{r}_i} \langle H \rangle, \quad (6)$$

with

$$\langle V_{ij} \rangle = \int d^3r d^3r' \phi_i^*(\mathbf{r}') \phi_j^*(\mathbf{r}) V(\mathbf{r}', \mathbf{r}) \phi_i(\mathbf{r}') \phi_j(\mathbf{r}). \quad (7)$$

These are the time evolution equations that are solved numerically. Note that the variational principle reduces the time evolution of the A_{tot} -body Schrödinger equation to the time evolution equations of $6(A_P + A_T)$ parameters to which a physical meaning can be attributed.

The nuclear dynamics of QMD model can also be translated into a semiclassical scheme. If one neglects the antisymmetrization, the Wigner distribution function f_i of the i th nucleon can be easily derived from the test wave function

$$\begin{aligned} f_i(\mathbf{r}, \mathbf{p}, t) = & \frac{1}{\pi^3 \hbar^3} \exp\{-[\mathbf{r} - \mathbf{r}_i(t)]^2(1/2L)\} \\ & \times \exp\{-[\mathbf{p} - \mathbf{p}_i(t)]^2(2L/\hbar^2)\} \quad (8) \end{aligned}$$

and the total one body Wigner density is the sum of those of all nucleons. The potential can be calculated with help of the wave function or of the Wigner density. Hence the expectation value of the total Hamiltonian reads

$$\langle H \rangle = \langle T \rangle + \langle V \rangle = \sum_i \frac{\mathbf{p}_i^2}{2m_i} + \sum_i \sum_{j>i} \int f_i(\mathbf{r}, \mathbf{p}, t) V^{ij} \times (\mathbf{r}', \mathbf{r}) f_j(\mathbf{r}', \mathbf{p}', t) d\mathbf{r} d\mathbf{r}' d\mathbf{p} d\mathbf{p}'. \quad (9)$$

Thus we neglect the finite width of the wave function in momentum space, which would add a constant term without changing the equations of motion. The baryon-baryon potential V^{ij} consists of the real part of the Brückner G matrix that is supplemented by an effective Coulomb interaction between the charged particles. The former can be further subdivided into a part containing the contact Skyrme-type interaction only and a contribution due to a finite range Yukawa potential. V^{ij} consists of

$$\begin{aligned} V^{ij}(\mathbf{r}' - \mathbf{r}) &= G^{ij} + V_{Coul}^{ij} = V_{Skyrme}^{ij} + V_{Yukawa}^{ij} + V_{Coul}^{ij} \\ &= t_1 \delta(\mathbf{r}' - \mathbf{r}) + t_2 \delta(\mathbf{r}' - \mathbf{r}) \rho^{\gamma-1} \left(\frac{\mathbf{r}' + \mathbf{r}}{2} \right) \\ &\quad + t_3 \frac{\exp(-|\mathbf{r}' - \mathbf{r}|/\mu)}{|\mathbf{r}' - \mathbf{r}|/\mu} + \frac{Z_i Z_j e^2}{|\mathbf{r}' - \mathbf{r}|}. \end{aligned} \quad (10)$$

The range of the Yukawa potential is chosen as 1.5 fm. Z_i and Z_j are the effective charges Z_p/N_p and Z_t/N_t of the i th and j th baryons. The real part of the Brückner G matrix is density dependent, which is reflected in the expression for G^{ij} . The expectation value of the Skyrme part of G for the i th nucleon is a function of the interaction density ρ_{int}^i

$$\begin{aligned} \rho_{int}^i(\mathbf{r}_i) &= \sum_{j \neq i} \int d^3 r d^3 r' \phi_i^*(\mathbf{r}') \phi_j^*(\mathbf{r}) \delta(\mathbf{r}' - \mathbf{r}) \phi_i(\mathbf{r}') \phi_j(\mathbf{r}) \\ &= \frac{1}{(\pi L)^{3/2}} \sum_{j \neq i} \exp[-(\mathbf{r}_i - \mathbf{r}_j)^2/L]. \end{aligned} \quad (11)$$

Note that the interaction density has twice the width of the single particle density $\rho^i(\mathbf{r}) = \phi_i^*(\mathbf{r}) \phi_i(\mathbf{r})$.

In infinite nuclear matter, the kinetic energy and potential interaction give rise to a nuclear equation of state of the form

$$E/N \left(\frac{\rho_{int}}{\rho_o} \right) = \frac{3}{5} E_{Fermi} \left(\frac{\rho_{int}}{\rho_o} \right)^{2/3} + U, \quad (12)$$

where the potential part resulting from the convolution of the distribution function f_i and f_j with the Skyrme interactions V_{Skyrme}^{ij} reads as

$$U = \alpha \left(\frac{\rho_{int}}{\rho_o} \right) + \beta \left(\frac{\rho_{int}}{\rho_o} \right)^\gamma. \quad (13)$$

Two of the three parameters of the equation of state are determined by demanding that at normal nuclear matter density, the binding energy should be equal to 16 MeV. The third one γ is usually treated as a free parameter. Its value is given in terms of the compressibility,

$$\kappa = 9\rho^2 \frac{\partial^2}{\partial \rho^2} \left(\frac{E}{A} \right). \quad (14)$$

For the present investigation, a soft equation of state corresponding to a compressibility κ of 200 MeV is employed. Then $\alpha = t_1 \rho_0 / 2 = -356$ MeV, $\beta = t_2 \rho_0^\gamma / (\gamma + 1) = 303$ MeV, and $\gamma = 1.17$. The parameters for the Yukawa potential are $t_3 = -6.66$ MeV and $\mu = 1.5$ fm. The stability and the binding energy of different fragments for this choice of parameters can be found in Ref. [5].

The imaginary part of the G matrix acts in a manner similar to a collision term. In QMD simulations, we restrict ourselves to binary collisions (two body level). The collisions are performed in a point-particle sense similar to the Vlasov-Uehling-Uhlenbeck or cascade calculations: two particles may collide if they come closer than $d_{min} = \sqrt{\sigma/\pi}$ where σ is a parametrization of the free nucleon-nucleon cross section. A collision does not take place if the final state phase space of the scattered particles is already occupied by particles of the same kind (Pauli blocking).

Neglecting antisymmetrization is a most drastic approximation of the model. In other words, all properties related to shell structures cannot be accounted for. The binding energy per nucleon follows the Weizsäcker mass formula. Hence, light fragments that show a large deviation from the Weizsäcker mass formula cannot be reproduced quantitatively. For the present study, the QMD version of Aichelin and co-workers has been used [5,17,18,21–27]. This present version has been tested extensively and has also been compared with the experimental findings.

III. RESULTS AND DISCUSSION

The time evolution of the nucleons is followed within the QMD model [5,18,21] and their phase space is stored at several time steps, which is then clusterized using the minimum spanning tree (MST) method that binds two nucleons in a fragment if their centroids are closer than 4 fm. Here we simulate the reactions with soft equation of state and standard energy dependent nucleon-nucleon cross section. In brief, we follow the time evolution of the nucleons till the end of the reaction which, in the present study, is 300 fm/c. The freeze-out time of 300 fm/c is much longer than a typical reaction time that is about 100 fm/c [5,21].

Here we simulate several thousand events involving the symmetric reactions like $^{40}\text{Ca} + ^{40}\text{Ca}$, $^{58}\text{Ni} + ^{58}\text{Ni}$, $^{93}\text{Nb} + ^{93}\text{Nb}$, $^{131}\text{Xe} + ^{131}\text{Xe}$, $^{168}\text{Er} + ^{168}\text{Er}$, $^{197}\text{Au} + ^{197}\text{Au}$, and $^{238}\text{U} + ^{238}\text{U}$ at incident energies between 50A MeV and 1A GeV and at different impact parameters $\hat{b} = b/b_{max}$; $b_{max} = R_1 + R_2$, $R_i = 1.48A^{(1/3)}$. The use of the symmetric nuclei simplifies the theoretical consideration and rescaled impact parameter \hat{b} assures the same geometrical overlap in all cases. By using the symmetric (colliding) nuclei, the system size effects can be analyzed without varying the asymmetry (and excitation energy) of the system. It is worth mentioning that the experimental studies by the MSU miniball and ALADiN [14,16] groups vary the asymmetry of the reaction whereas the plastic ball [11] and FOPI experiments

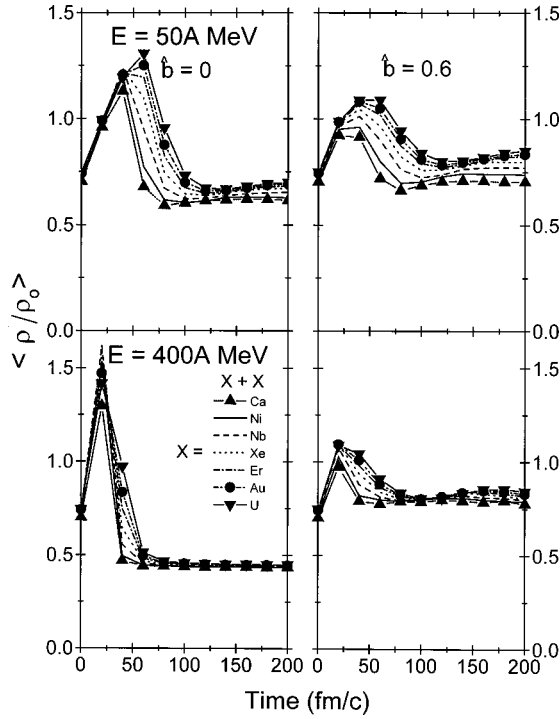


FIG. 1. Average density $\langle \rho / \rho_0 \rangle$ as a function of the time. Here the density is calculated using Eq. (15). The top panel is at 50 MeV/nucleon, whereas the bottom panel represents the reaction at 400 MeV/nucleon. The left- and right-hand sides represent, respectively, the central collision $\hat{b}=0$ and peripheral collision $\hat{b}=0.6$. All the reactions are for symmetric colliding nuclei $X+X$, where X represents the Ca (filled triangle), Ni (solid line), Nb (dashed line), Xe (dotted line), Er (dashed-dotted line), Au (solid circle and dashed-double-dotted line), and U (inverted triangle).

[12] are performed for symmetric reactions. In the following, we first discuss the time evolution of different reactions and, then, shall present the relative dependence of the multiplicity of different fragments on the size of the interacting system.

a. Time evolution. The nucleonic density and the frequency of nucleon-nucleon collision are related to the breaking of nuclei into fragments. It is, therefore, important to study the evolution of the density and nucleon-nucleon collisions. We display in Fig. 1, the average density of the reaction, which is calculated as [18,22]

$$\langle \rho \rangle = \left\langle \frac{1}{A_T + A_P} \sum_{i=1}^{A_T + A_P} \sum_{j=1}^{A_T + A_P} \frac{1}{(2\pi L)^{3/2}} \times \exp\left[-\frac{[\mathbf{r}_i - \mathbf{r}_j]^2}{2L}\right] \right\rangle, \quad (15)$$

with \vec{r}_i , and \vec{r}_j , respectively, the position coordinates of i th and j th nucleons. In Fig. 1, we show the evolution of the density $\langle \rho / \rho_0 \rangle$ at two typical incident energies 50 and 400 MeV/nucleon and at two impact parameters $\hat{b}=0$ and 0.6. The central collisions (at low incident energies) as well as the peripheral collisions (at all incident energies) lack the frequent nucleon-nucleon collisions and, therefore, most of

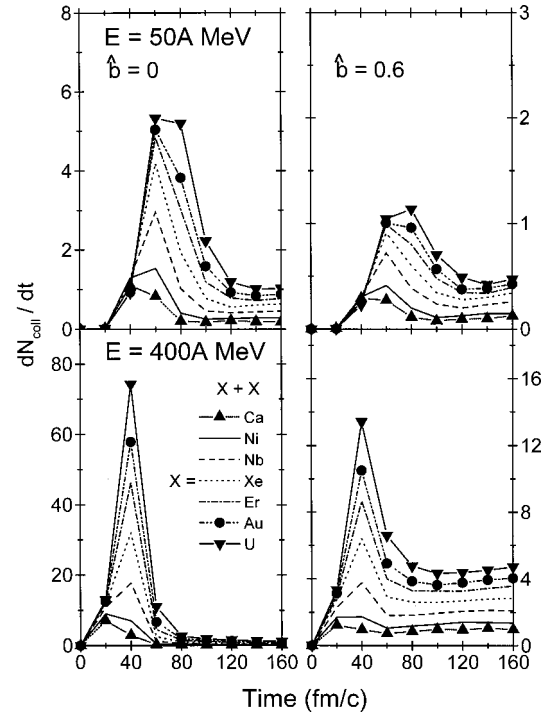


FIG. 2. Same as Fig. 1, but for the rate of collision dN_{coll}/dt .

the initial memories of the nucleons (and the correlations among them) are preserved. In contrast, the frequent occurrence of the nucleon-nucleon collisions at central higher incident energies destroys most of the correlation among them. If one goes beyond 400 MeV/nucleon, little change occurs in fragment's structure [12,13,16,23]. From Fig. 1, we see that the heavier colliding nuclei are more compressed compared to the lighter one. In addition, the dense (and hot) matter exists longer in the heavier colliding nuclei compared to the lighter nuclei. It is worth mentioning that the maximum temperature is unaffected by the size of the system, whereas the density (both the maximum and average) in central region depends on the size of the system [2,3,14]. After the compression, the matter expands and breaks into fragments (consisting of the entities of all sizes). As the higher compression exists longer for the heavy nuclei, one would expect a delayed triggering of the multifragmentation in these reactions. Note that the higher density ($\langle \rho / \rho_0 \rangle \geq 1$) at 50 MeV/nucleon remains till about 75 fm/c for U+U reaction compared to 40 fm/c for Ca+Ca reaction. In other words, the excited heaviest fragment A^{max} (detected in the MST method) will remain for a longer time. A large freeze-out density (at 200 fm/c) for heavier masses indicates the existence of the heavier fragments. On the other hand, one should expect universality beyond 400 MeV/nucleon.

The preservation of the initial nucleon-nucleon correlations can be linked with the collision rate that is displayed in Fig. 2. Naturally, the peripheral collisions have lesser overlap and hence lesser collision rate. Due to (available) free phase space at higher incident energies, the collision rate is very high. We also notice that the maximum collision rate for central U+U system (at 400 MeV/nucleon) is about 74, whereas it is 5.3 at 50 MeV/nucleon. Similar evolution can

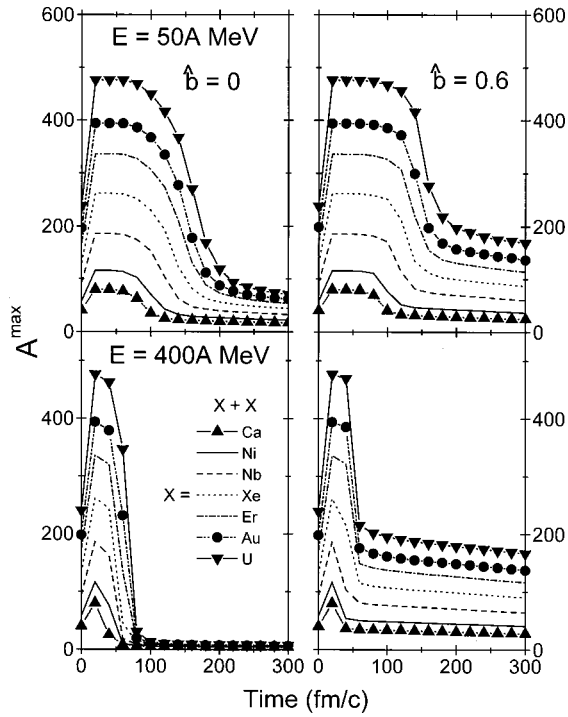


FIG. 3. Same as Fig. 1, but for the time evolution of the heaviest fragment A^{\max} as a function of the time.

also be seen at peripheral geometry. The trends of the collision rate and density are quite similar. The maximal collision rate, which lasts longer in heavier colliding nuclei, will not allow the fragment distribution to saturate for long time. In other words, the saturation time of the fragmentation yield will be shorter in lighter systems compared to heavy systems. The finite collision rate at freeze-out time points towards the compactness of the nuclear matter.

The time evolution of the formation of fragments gives insight into the cause of fragmentation and reaction dynamics. In Figs. 3–5, we show the time evolution of different fragments. The time evolution of the heaviest fragment A^{\max} , emitted nucleons, and medium mass fragments MMF's ($5 \leq A \leq 9$) is displayed, respectively, in Figs. 3, 4, and 5. The displayed MMF's exclude the heaviest fragment and, therefore, are represented by MMF's*. The top panel in all figures is at 50 MeV/nucleon, whereas the bottom panel is at 400 MeV/nucleon. As expected from Fig. 1 (where the evolution of the density was shown), the A^{\max} last longer in heavier systems compared to lighter systems. The excited A^{\max} in heavier systems continues to emit the nucleons till the end of the reaction, whereas it saturates around 100 fm/c in light systems indicating the cold and separated matter. The emission of the nucleons (shown in Fig. 4) reflects the same trend. Due to finite collision rate (in heavier colliding nuclei), the emission of the nucleons and light charged particles continues till the end of reaction. Note that the saturation for central collisions occurs around 80 fm/c in Ca+Ca system, whereas it takes 250 fm/c for U+U system. The saturation of the free nucleons occurs earlier at higher incident energies, which indicates a faster disintegration of the matter at these energies. The time evolution of the

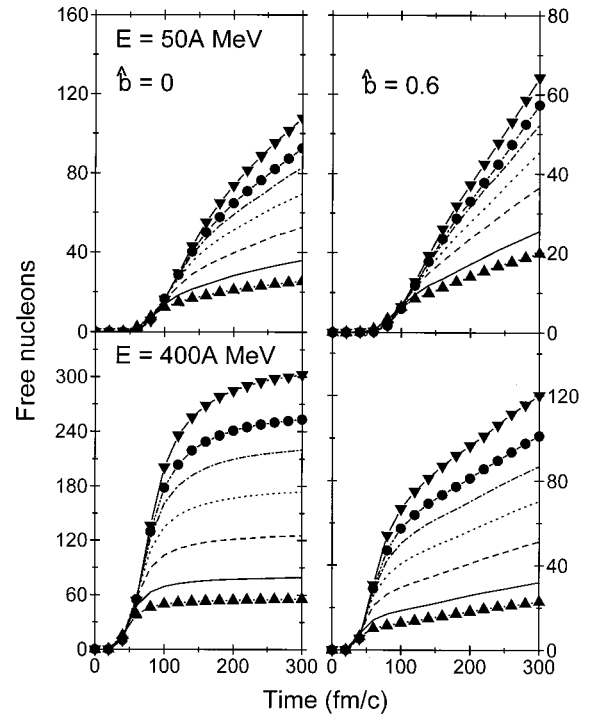


FIG. 4. Same as Fig. 1, but for the time evolution of the multiplicity of free particles.

light charged particles ($2 \leq A \leq 4$) (not shown here) also follows a similar trend.

On the other hand, the formation of the MMF's* (Fig. 5) has a different evolution. While the MMF's* at 50 MeV/nucleon are stable and saturate around 120–200 fm/c, the

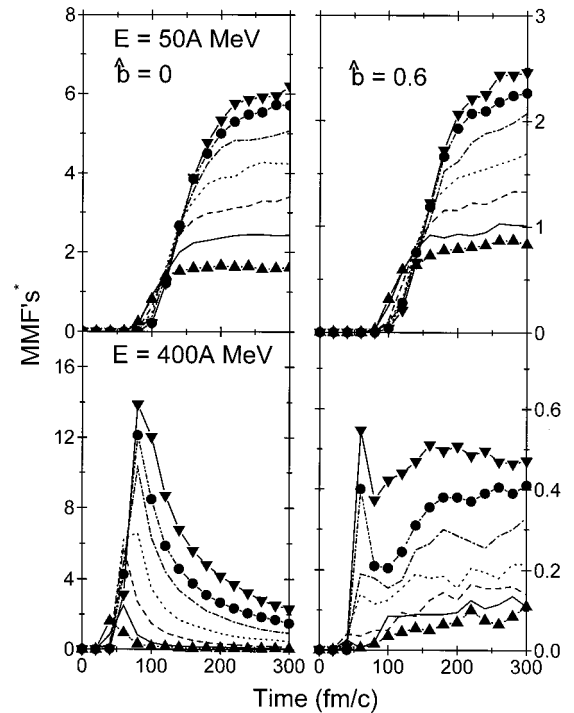


FIG. 5. Same as Fig. 1, but for the time evolution of the medium mass fragment MMF's*.

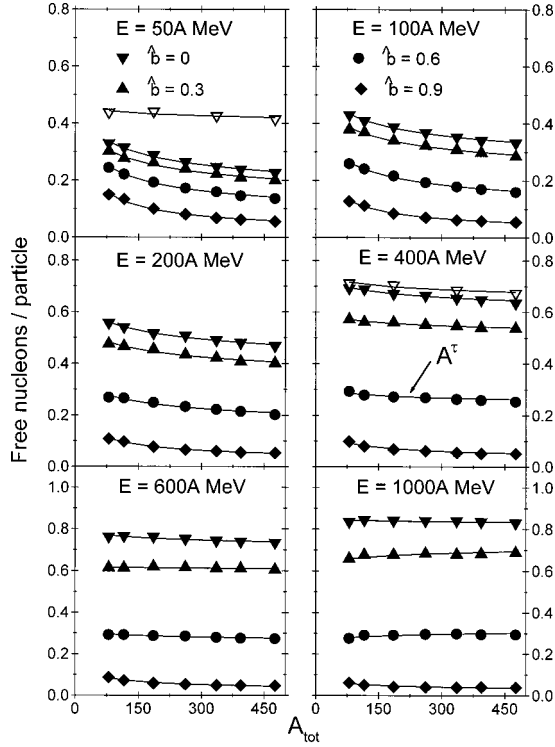


FIG. 6. Final state multiplicity (calculated at 300 fm/c) of the free particles per nucleon as a function of the composite mass of the system A_{tot} ($=A_T + A_P$; A_T and A_P are, respectively, the mass of the target and projectile). The left-hand side of the top, middle and bottom panels represents, respectively, the reaction at 50, 200, and 600 MeV/nucleon. The right-hand side of the top, middle, and bottom panels represents, respectively, the reaction at 100, 400, and 1000 MeV/nucleon. In each window, four symbols, i.e., the inverted triangle, triangle, solid circle, and diamond represent, respectively, the reaction at $\hat{b} = 0, 0.3, 0.6,$ and 0.9 . The open symbols show the results at 800 fm/c. All curves are using $y = cA_{tot}^\tau$.

MMF's* in central 400 MeV/nucleon are very excited and unstable, which continuously emit the light fragments/particles. Again the saturation time is much shorter for lighter system. These results are in agreement with the earlier calculations [18]. One also notices that the triggering of the fragmentation is delayed in heavier colliding nuclei compared to lighter nuclei. If one plots the final state multiplicity of the MMF's* as a function of the impact parameter, one will observe the well known rise and fall of the multiplicity [18].

The above findings show that the light mass fragments are formed at a very early stage of the reaction. The light charged particles ($2 \leq A \leq 4$) do not decay and seem to be originating from the surface of the confined system at higher incident energies. These fragments measure the violence of the reaction, therefore, depend on the impact parameter. We have also checked the binding energy of different fragments produced in the above reactions and find that they are properly bound at the end of the reaction.

b. Final state distribution. Naturally, experimental measurements are done at the end of the reaction. Therefore, it will be of interest to see whether the final fragment's distri-

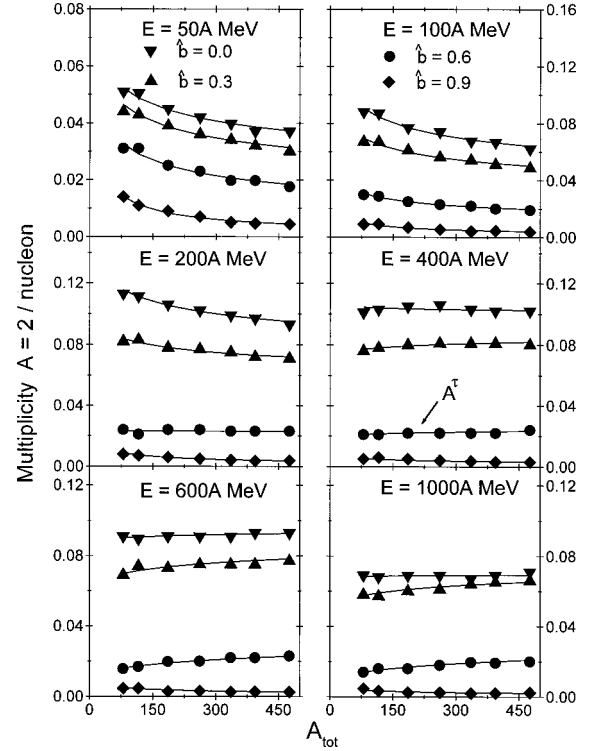


FIG. 7. Same as Fig. 6, but for the final state multiplicity of the fragments with mass=2.

bution of different reactions can be related to the size of the system or not.

We display in Figs. 6–10, the reduced multiplicity (multiplicity per nucleon) of the free nucleons as well as of the fragments with mass $A = 2$, LMF's, MMF's, and MMF's*. Note that in contrary to the FOPI and ALADiN experiments, we do not divide the matter into participant and spectator zones. The top panel in each figure displays the multiplicities at 50 and 100 MeV/nucleon, whereas the bottom panel is at 600 MeV/nucleon and 1000 MeV/nucleon. The middle panel represents the 200 and 400 MeV/nucleon. The windows in each panel contain four different curves that correspond, respectively, to the scaled impact parameter values of $\hat{b} = 0.0, 0.3, 0.6,$ and 0.9 . First of all, the wide range of the incident energy between 50 MeV/nucleon and 1000 MeV/nucleon and impact parameter between zero and b_{max} deals with different dynamics emerging at low, intermediate, and high energies. The nature of the dynamics at low energy is more of a fusion-fission, whereas the multifragmentation dominates the scenario at medium energies. At higher incident energies, one has complete disassembly of the nuclear matter, which makes the multifragmentation a rare process. The central collisions lead to the participant matter dynamics, whereas the dynamics at peripheral geometries is more of a spectator physics. The Fermi spheres of the projectile and target become separated at incident energies of about 50–100 MeV/nucleon and hence, one may expect that it is the beginning of the transition regime between the low-energy-heavy-ion reactions, demanded by the compound nucleus formation and the high-energy-heavy-ion reaction where a clear participant-spectator picture emerges.

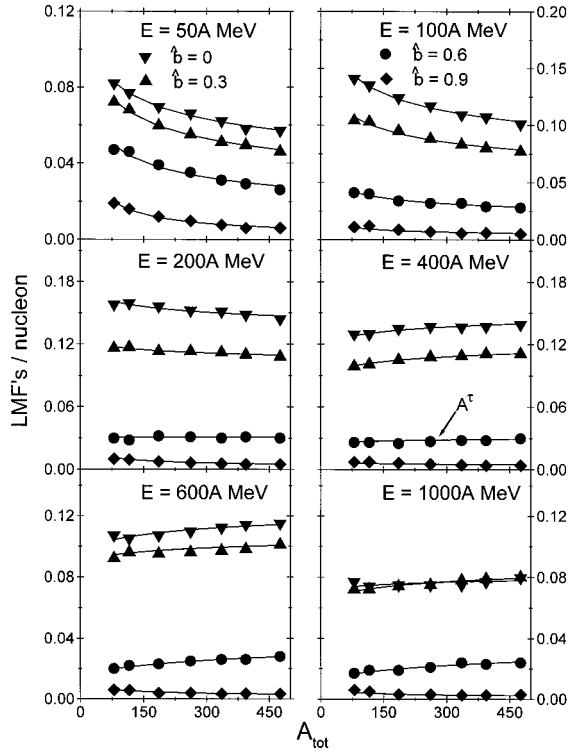


FIG. 8. Same as Fig. 6, but for the final state multiplicity of LMF's.

As discussed above, the general behavior of all light mass fragments follows the well known trends. In peripheral collisions, the geometry is dominated by the spectator physics. The free nucleons as well as the light charged particles scale with the size of the participant matter. Their multiplicity is maximum for the central collisions, which decreases with an increase in the impact parameter. One also sees that the number of the emitted nucleons and light mass fragments ($A \leq 4$) increases with the incident energy. At higher incident energies, most of the initial nucleon-nucleon correlations are destroyed in participant matter and, therefore, only light particles survive from the reaction zone. In contrast, due to large Pauli blocking at low incident energies, many nucleons in the reaction zone survive the reaction without suffering the collisions with large momentum transfer. The energy received by the target in peripheral collisions is not enough to excite the matter far above the Fermi level, resulting in fewer light fragments. In other words, the emission of the heavier fragments becomes more and more a phenomena of peripheral collision with the increase in the incident energy. To deal with this situation, the FOPI [12] and ALADiN groups [16] divided the nuclear matter into spectator and participant zone. Our present interest lies in the light mass fragments (with mass less than 10), therefore, we do not divide the matter into the participant and spectator zones.

Remarkably, independent of the mass of the fragments as well as the incident energy and impact parameter, the multiplicity of any kind of fragment (i.e., of free nucleons, fragments with masses $A=2$, $2 \leq A \leq 4$, and $5 \leq A \leq 9$) scales with the size of the system that can be parametrized by a power law of the form cA_{tot}^τ ; A_{tot} is the composite mass of

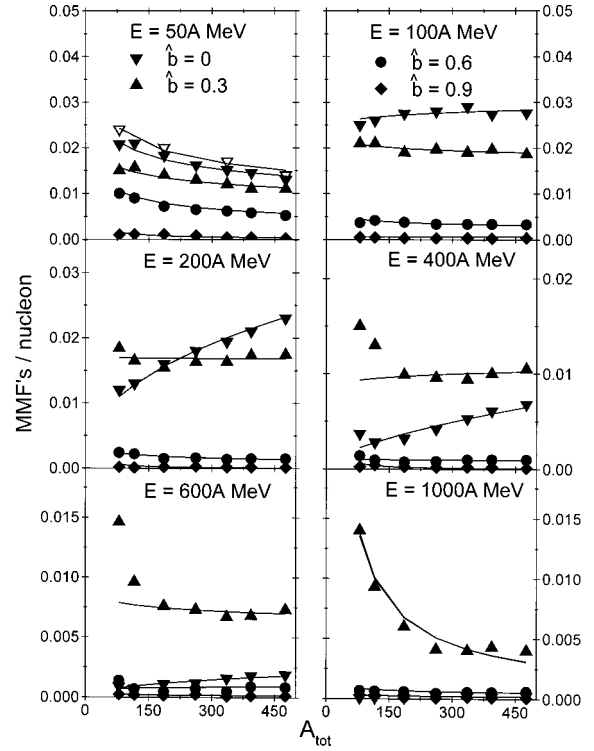


FIG. 9. Same as Fig. 6, but for the MMF's.

the system. The values of the constants c and τ depend on the size of the fragments as well as on the incident energy and impact parameter [17]. This dependence of τ will be discussed in the following paragraphs. We have also tried a functional form $c e^{-\tau A}$. The fits were, however, worse than the one obtained with power law.

A word of caution should be added here: It has been shown and discussed extensively in the literature that the mass yield curve approximately obeys a power law behavior $\propto A_{frag}^{-\tau}$ [24]. It has been conjectured (though controversial) that this behavior (which has also been termed as “accidental” [21]) is an indication of the phase transition between a gaseous and a liquid phase of the nuclear matter. Note that the said power law behavior of the mass (or charge) distribution is for a “given system” [24]. The above power law dependence, which we are discussing, is something very different. The above power law function is for the multiplicity of a “given fragment” that scales with the size of the system. The existence of the above power law dependence at impact parameters and incident energies indicates the universality of the power law behavior for the system size effect in the production of light mass fragments.

From Fig. 6, we also notice that the percentage of the free particles increases drastically with the incident energy, which can be as high as 80% for central collision. If we label the reaction above 60% or more free particle as total disassembly, we see a clear disassembly of the matter in central collision above 400 MeV/nucleon.

From Figs. 6–10, we see a maximum effect (of system size) at low incident energies, which decreases with incident energy. The emission of the light charged particles exhibits linear dependence at higher incident energies. One of the

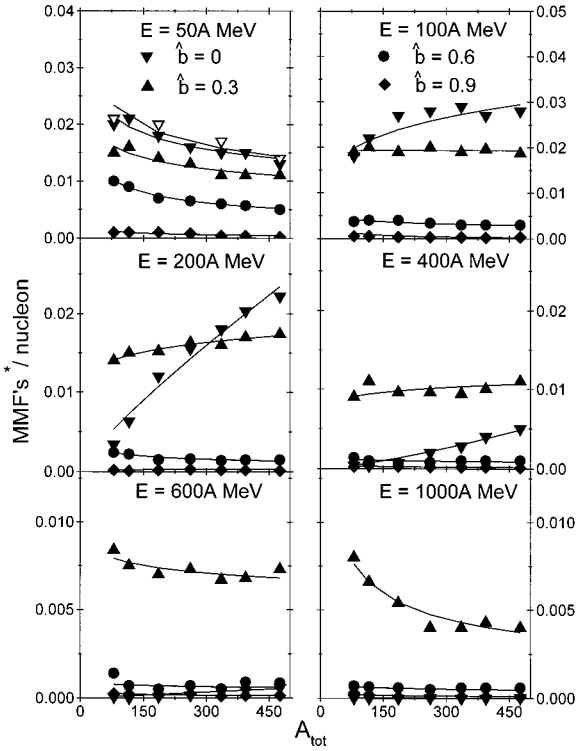


FIG. 10. Same as Fig. 9, but for the MMF's excluding the heaviest fragment A^{max} (denoted by MMF's*).

possible causes of this sharp dependence is the late saturation in heavier colliding nuclei (see, e.g., Fig. 4). From Fig. 4, we see that the multiplicity of the free nucleons and light charged particles in lighter colliding nuclei saturates around 200 fm/c, whereas it takes a much longer time for heavier nuclei. As our nuclei are stable for a typical time span of 300 fm/c, we cannot follow the reaction beyond this time. If we analyze the mass dependence at a later stage, the multiplicity is likely to be changed for heavy systems. To demonstrate this, we show the outcome of various fragments at 800 fm/c (dashed lines). We see that the particle emission in heavier nuclei changes drastically beyond 300 fm/c at low incident energies, whereas nearly no effect exists at higher incident energies. The multiplicity of the light charged particles does not change.

Our results (at 400 MeV/nucleon) are in agreement with Ref. [11] where the normalized charge was reported to decrease from Ca+Ca to Au+Au. In contrary to the light charged particles, the multiplicity of the MMF's* (Fig. 9) has a sharp dependence on the size of the system in some cases. If we look at Fig. 3 (where the size of the heaviest fragment is displayed), we find that the size of A^{max} in many cases is quite close to the range of the MMF's ($5 \leq A \leq 9$). In order to strengthen our argument, we show, in Fig. 10, the multiplicity of MMF's excluding the A^{max} (marked by MMF's*). Once the A^{max} is excluded, the sharp dependence of the MMF's on the size of system washes away in most of the cases. This happens due to the fact that the A^{max} [which is close to the extreme limits of the MMF's (either 5 or 9)] will be included sometime whereas it may be excluded other times that makes a sharp system size dependence.

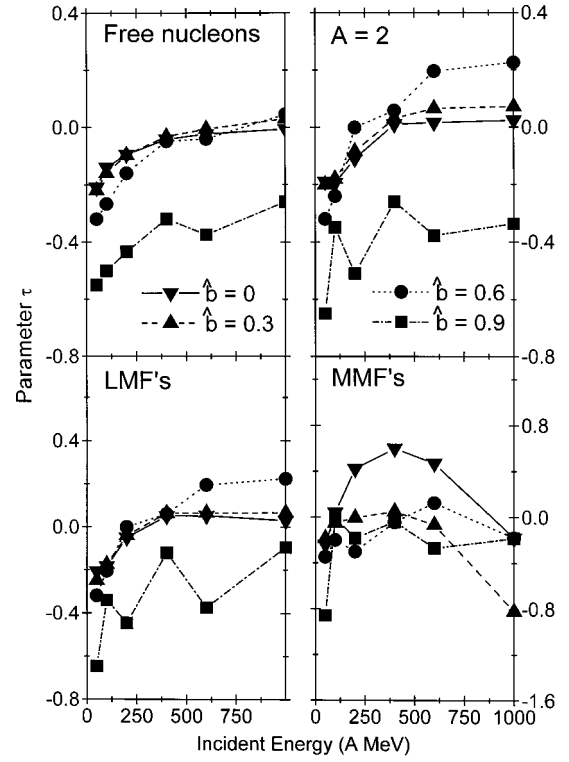


FIG. 11. Parameter τ (appearing in the power law function A_{tot}^{τ}) as a function of the incident energy. The top panel displays the values of τ for free nucleon (left part) and fragments with mass equal to 2 (right part). The bottom panel represents the values of τ for LMF's (left panel) and MMF's (right panel). The different symbols, namely, the inverted triangle, triangle, solid circle, and square, represent the results at impact parameter $\hat{b} = 0, 0.3, 0.6, \text{ and } 0.9$.

It is worth mentioning that if one plots the reported results of the FOPI experiments [12] as a function of the size of the system, a similar power law fit can also be obtained. Note that the analysis of the FOPI experiments [12] has been done for the participant zone only. Our present calculations include both the participant and spectator zones. As discussed above, similar power law dependencies have also been reported for other observables. For example: the probability of the kaon production was reported to depend on the size of the system and was parametrized in terms of a power law function [7]. A similar power law dependence was also obtained for the collective flow. The different slopes of the power law at low and higher incident energies can be coupled with the collective flow that depends on the incident energy as well as on the mass of the system.

The τ dependence as a function of the incident energy is displayed in Fig. 11. The different symbols in the figure represent different impact parameters. We do not see any unique value of the τ . For the central collisions, the value of the parameter τ is close to $1/3$ at 50 MeV/nucleon that first increases with the incident energy and then finally saturates at very high incident energy. In other words, the total multiplicity of the fragments will be $= A \times A^{-1/3} = A^{2/3}$, which is like a surface of the colliding nuclei representing the mean field. Therefore, it seems that the mass dependence at low incident energies is similar to that of a mean field. With the increase

in the incident energy, the value of the parameter τ tends to approach zero (the unscaled value will be ≈ 1). This corresponds to a linear dependence. It has been stated by a number of authors that the repulsive nucleon-nucleon interactions at high energies scale like A [10]. Unlike the disappearance of flow (which rescales as $A^{-1/3}$ [10]), the present τ dependence is not unique. It is worth mentioning that the power law factor τ in kaon production also depends on the incident energy as well as on the equation of state one is using. As reported by Hartnack *et al.* [7] no unique dependence of τ could be obtained for the kaon production.

IV. SUMMARY

Using the quantum molecular dynamics (QMD) model coupled with the minimum spanning tree (MST) method, we investigated in detail the formation of various light mass fragments and their dependence on the size of the system. For detailed analysis, we studied the reactions at incident energies between 50 and 1 GeV/nucleon and over full geometrical overlap using symmetric colliding nuclei with mass between 40 and 238. As we know, the ratio of the surface to volume decreases with the size of the system, whereas the compressional effects increase. The lighter colliding nuclei generate less density, whereas a higher density is achieved with heavy nuclei, which gives ample space for compression depression as well as radial expansion.

The system-size effects depend on the reaction inputs as well as on the colliding geometries. The multiplicity of any kind of fragment can be parametrized in terms of a power law $\propto A_{tot}^\tau$, where A_{tot} is the total mass of the composite system. This is true for a wide range of the impact parameter

and incident energy considered here. However, the parameter τ does not have a unique value. Rather, it seems that the parameter τ is close to $2/3$ at lower energies suggesting the dominance of the mean field that scales as $A^{2/3}$. In contrast, we obtain a nearly linear dependence at higher incident energies suggesting the dominance of the repulsive scattering at higher incident energies. Similar system-size power law dependence has also been reported in other observables like in the disappearance of flow [10] as well as in the production of kaon/pion [7] and in low incident energy phenomena, such as, the fusion, etc. [1]. Such trends can also be seen in the preliminary experimental results of FOPI group that has measured the intermediate mass fragment yields [12].

It is worth mentioning that the results of the multifragmentation are found to be sensitive towards the different model ingredients, such as, the equation of state (with/without momentum dependent interactions [25] and nucleon-nucleon cross section [26]) as well as towards the clusterization method one is using [27]. As has been reported in the literature, the MST method does not yield proper results at higher incident energies, whereas a more sophisticated model can yield better results [22]. In view of these points, we would like to add that the value of parameter τ may depend on the model ingredients one is using. Its value may change with the method/input, but the power law dependence of the system-size effect should exhibit.

ACKNOWLEDGMENT

This work was supported by the grant from Department of Science and Technology (DST) Government of India vide Grant No. SP/S2/K-21/96.

-
- [1] L.C. Vaz, J.M. Alexander, and G.R. Satchler, *Phys. Rep.* **69**, 373 (1981); M. Beckerman, *Rep. Prog. Phys.* **51**, 1047 (1988); J. Blocki, J. Randrup, W.J. Swiatecki, and C.F. Tsang, *Ann. Phys. (N.Y.)* **105**, 427 (1977); J. Blocki and W.J. Swiatecki, *ibid.* **132**, 53 (1981); R. K. Puri, Ph.D. thesis, Panjab University, Chandigarh, 1990.
- [2] D.T. Khoa, N. Ohtsuka, A. Faessler, M.A. Matin, S.W. Huang, E. Lehmann, and Y. Lofty, *Nucl. Phys.* **A542**, 671 (1992); D.T. Khoa, N. Ohtsuka, M.A. Matin, A. Faessler, S.W. Huang, E. Lehmann, and R.K. Puri, *ibid.* **A548**, 102 (1992).
- [3] R.K. Puri, N. Ohtsuka, E. Lehmann, A. Faessler, M.A. Matin, D.T. Khoa, G. Batko, and S.W. Huang, *Nucl. Phys.* **A575**, 733 (1994); R. K. Puri, E. Lehmann, N. Ohtsuka, Amand Faessler, and S. W. Huang, in *Proceedings of the International Workshop XXII on Gross Properties of Nuclei and Nuclear Excitations*, Hirschegg, Austria, 1994, edited by H. Feldmeier, p. 262; R.K. Puri, J. Singh, J. Aichelin, and A. Faessler, in *Horizon of Physics*, edited by R.K. Gupta (Narosa, New Delhi, India).
- [4] C. Hartnack, GSI Report No. 93, 1993 (unpublished).
- [5] J. Aichelin, *Phys. Rep.* **202**, 233 (1991).
- [6] C. Sturm *et al.*, *Phys. Rev. Lett.* **86**, 39 (2001).
- [7] C. Hartnack, J. Jaenicke, L. Sehn, H. Stöcker, and J. Aichelin, *Nucl. Phys.* **A580**, 643 (1994).
- [8] K.G.R. Doss *et al.*, *Phys. Rev. C* **32**, 116 (1985); **37**, 163 (1988).
- [9] W. Reisdorf and H.G. Ritter, *Annu. Rev. Nucl. Part. Sci.* **47**, 663 (1997).
- [10] G.D. Westfall *et al.*, *Phys. Rev. Lett.* **71**, 1986 (1993); V. de La Mota *et al.*, *Phys. Rev. C* **46**, 677 (1992); E. Lehmann, A. Faessler, J. Zipprich, R.K. Puri, and S.W. Huang, *Z. Phys. A* **355**, 55 (1996); D.J. Magestro *et al.*, *Phys. Rev. C* **61**, 021602(R) (2000); R. Pak *et al.*, *ibid.* **53**, R1469 (1996).
- [11] H.H. Gutbrod, K.H. Kampert, B.W. Kolb, A.M. Poskanzer, H.G. Ritter, and H.R. Schmidt, *Z. Phys. A* **337**, 57 (1990).
- [12] B. de Schauenburg *et al.*, GSI Rep. No. 98-1, 1997 (unpublished); G. S. Wang *et al.*, *ibid.* 96-1, 1995 (unpublished); 97-1, 1996 (unpublished); W. Reisdorf *et al.*, *ibid.* 2000, 1999 (unpublished); W. Reisdorf, in *Proceedings of the International Workshop XXVII on Gross Properties of Nuclei and Nuclear Excitations*, Hirschegg, Austria, 1999, edited by H. Feldmeier, J. Knoll, W. Noerenberg, and J. Wambach, p. 82; W. Reisdorf, *Nucl. Phys.* **A630**, 15c (1998).
- [13] J. Konopka *et al.*, GSI Rep. 96-1, 1995 (unpublished); J.P. Alard *et al.*, *ibid.* 97-1, 1996 (unpublished); N. Bastid *et al.*, *ibid.* 98-1, 1997 (unpublished); A. Andronic *et al.*, *ibid.* 98-1, 1997 (unpublished).

- [14] D.R. Bowman *et al.*, Phys. Rev. C **46**, 1834 (1992).
- [15] E. Piasecki, *et al.*, Phys. Rev. Lett. **66**, 1291 (1991).
- [16] A. Schüttauf *et al.*, Nucl. Phys. **A607**, 457 (1996); M. Bagemann-Blaich *et al.*, Phys. Rev. C **48**, 610 (1993); M.B. Tsang *et al.*, Phys. Rev. Lett. **71**, 1502 (1993).
- [17] J. Singh, S. Kumar, and R.K. Puri, DAE Sym. **41B**, 258 (1998); J. Singh and R.K. Puri, Phys. Lett. B (to be published).
- [18] R.K. Puri and S. Kumar, Phys. Rev. C **57**, 2744 (1998); J. Singh, S. Kumar, and R.K. Puri, *ibid.* **62**, 044617 (2000); J. Singh and R.K. Puri, *ibid.* **62**, 054602 (2000); J. Singh, S. Kumar, and R.K. Puri, *ibid.* **63**, 054603 (2001).
- [19] J.P. Bondorf, R. Donangelo, I.N. Mishutin, and H. Schulz, Nucl. Phys. **A444**, 460 (1985).
- [20] W. Bauer, G.F. Bertsch, and H. Schulz, Phys. Rev. Lett. **69**, 1888 (1992).
- [21] A. Bohnet, J. Aichelin, P. Pochodzalla, W. Trautmann, G. Peilert, H. Stöcker, and W. Greiner, Phys. Rev. C **44**, 2111 (1991); G. Peilert *et al.*, *ibid.* **39**, 1402 (1989); Ch. Hartnack, R.K. Puri, J. Aichelin, J. Konopka, S.A. Bass, H. Stöcker, and W. Greiner, Eur. Phys. J. A **1**, 151 (1998); R. Nebauer *et al.*, Nucl. Phys. **A658**, 67 (1999); J. Konopka, Ph.D. thesis, Frankfurt University, Frankfurt, 1995; L. Zhuxia, C. Hartnack, H. Stöcker, and W. Greiner, Phys. Rev. C **44**, 824 (1991).
- [22] R.K. Puri, C. Hartnack, and J. Aichelin, Phys. Rev. C **54**, R28 (1996); R.K. Puri and J. Aichelin, J. Comput. Phys. **162**, 245 (2000); P.B. Gossiaux, R.K. Puri, Ch. Hartnack, and J. Aichelin, Nucl. Phys. **A619**, 379 (1997).
- [23] N. Marie *et al.*, Phys. Rev. C **58**, 256 (1998); J. Lukasik *et al.*, *ibid.* **55**, 1906 (1997); C.A. Ogilvie *et al.*, Phys. Rev. Lett. **67**, 1214 (1991); G.F. Peaslee *et al.*, Phys. Rev. C **49**, R2271 (1994); K. Hagel *et al.*, Phys. Rev. Lett. **68**, 2141 (1992); N.T.B. Stone *et al.*, *ibid.* **78**, 2084 (1997); J. Hubble *et al.*, Phys. Rev. C **46**, R1577 (1992); J. Hubble *et al.*, Z. Phys. A **340**, 263 (1991).
- [24] T. Li *et al.*, Phys. Rev. Lett. **70**, 1924 (1993); Y.G. Ma and W.Q. Shen, Phys. Rev. C **51**, 710 (1995).
- [25] S. Kumar and R.K. Puri, Phys. Rev. C **60**, 054607 (1999).
- [26] S. Kumar, R.K. Puri, and J. Aichelin, Phys. Rev. C **58**, 1618 (1998); C. Roy *et al.*, Z. Phys. A **358**, 73 (1997).
- [27] S. Kumar and R.K. Puri, Phys. Rev. C **58**, 2858 (1998); **58**, 320 (1998).